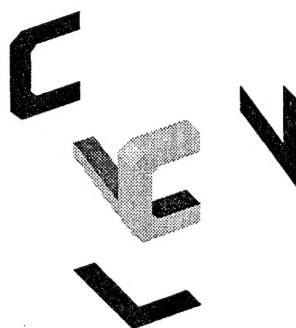


COMPUTER VISION LABORATORY



DTIC QUALITY INSPECTED 4

CENTER FOR AUTOMATION RESEARCH

UNIVERSITY OF MARYLAND
COLLEGE PARK, MARYLAND
20742-3275

19960212 011

CAR-TR-784
CS-TR-3509

DAAH04-93-G-0419
August 1995

Off-Road Navigation from Selective Stabilization

Y.S. Yao
R. Chellappa

Computer Vision Laboratory
Center for Automation Research
University of Maryland
College Park, MD 20742-3275

Abstract

This paper studies the problem of selective stabilization, defined here as the separation of rotation components due to smooth rotation and oscillatory rotation. In applications to off-road navigation, in addition to the desired smooth attitude change, a vehicle undergoes high frequency vibration. We consider both kinematic and kinetic models suitable for capturing these phenomena and achieving their separation. Our approach uses various dynamic laws to model the behavior of the vehicle, and relies on Extended Kalman Filters for the estimation. Multiple visual cues are exploited to obtain the rotational parameters. A scheme for detecting the occurrence and disappearance of smooth rotation is devised. Appropriate dynamic laws are employed to achieve selective stabilization. Based on the selective stabilization, 3-D locations of close feature points are estimated in a stabilized frame of reference, thus providing more useful information. Synthetic experiments for different scenarios using the proposed approach show promising results.

Keywords: Selective stabilization, motion analysis, structure from selective stabilization, kinematic and kinetic models

1 Introduction

Vision has been an important factor in intelligent mobile robotics. In order to move around the environment, knowledge about a robot's motion and relevant structures in the environment is essential. Many related tasks such as moving object detection, obstacle avoidance, and target acquisition also become easier when this information is available. Numerous approaches to these problems have been proposed. Depending on their inputs, major techniques are typically either flow-based or feature-based.

Under the assumption that the optical flow is identical to the motion field, flow-based methods employ spatial and temporal image gradients to infer motion and structure. Since only flow components in the directions of image gradients can be computed directly, additional constraints are introduced in recovering the optical flow [8, 10, 11, 16]. Then, based on the computed optical flow, motion and structure are extracted [1, 14, 19]. Alternatively, direct estimation of motion and structure, without computing the optical flow, have also been pursued [9, 17]. Although great advances have been made, instability and sensitivity to noise in estimating image derivatives limit flow-based methods to application only in situations where the image sequence is dense, while the inter-frame motion is also small.

Feature-based techniques use a set of discrete features such as points or lines to extract information. As in many flow-based approaches, the first step is to solve a correspondence problem, i.e. to determine corresponding features over the sequence. The motion and structure are then recovered in the next step. Much of the early work using this approach focused on using two or three frames, resulting in simple linear algorithms [13, 18]. However, a lack of robustness of the estimates to correspondence errors has been observed [2, 6]. One way in which robust algorithms can be obtained is by exploiting the dynamic nature of the sequence.

We are interested in studying dynamic laws suitable for capturing the behavior of mobile robots, especially for off-road navigation applications. Since the translation of a vehicle is mainly along its longitudinal axis and its speed can easily be obtained from the odometer, we concentrate on dynamic laws for describing the rotation of a vehicle. The orientation of a vehicle, in general, is determined by a desired smooth rotation and an undesired high frequency oscillatory rotation. The smooth rotation is defined here as the attitude change of the vehicle arising from the steering commands and/or the effect of following a smooth surface. The oscillatory rotation, on the other hand, is typically the response of mechanical elements to roughness components in natural terrain.

In applications such as teleoperation, it is desirable to provide the impression of smooth rotation (such as arises in steering and climbing) to the teleoperator, while removing non-smooth rotation. Additional sensors such as gyros and accelerometers could be used to compensate for these effects. However, this could result in a prohibitively costly system. The possibility of separating the two types of rotations directly from the images is therefore of interest. We refer to this procedure as *selective stabilization*.

To achieve selective stabilization, we first consider the recovery of parameters relevant to the total rotation, which is the sum of smooth rotation and oscillatory rotation. This process is called image stabilization. Image plane displacements of distant feature points may unambiguously characterize total rotational motion. However, such points are sometimes difficult to detect and track, due to the absence of sufficient intensity gradient information. Horizon lines, when present, constitute very strong visual cues, requiring relatively simple operations for their tracking. These tokens are therefore used to estimate the total rotation parameters.

We then seek to separate smooth rotation and oscillatory rotation. Assuming that the attitude of the vehicle varies smoothly, a kinematic law is employed to model the behavior of the corresponding smooth rotation parameters. The oscillatory rotation is captured by a kinetic model. A four-wheel vehicle model used in the design of suspension systems is considered for this purpose. In some situations, parts of the smooth rotation and oscillatory rotation are not coupled. For example, if high frequency yaw motion is negligible, steering directly corresponds to a component of total rotation. Similarly, if the banking behavior of the vehicle is not considered, roll motion is directly observable from the total rotation. Consequently, only the climbing and pitch motions are coupled. Furthermore, climbing does not occur at all times. We therefore design a detection scheme for the occurrence and disappearance of climbing. Based on the detection results, the selective stabilization algorithm is adjusted accordingly.

Another issue concerns estimation of the relative positions of close scene points with respect to the vehicle. Much of the earlier work estimates these positions without considering the effect of oscillatory rotation. Decisions or actions based on the resulting estimates may be inappropriate. If selective stabilization can be achieved, we can estimate the 3-D locations of a set of close features in a desirable frame of reference, which is less perturbed by the oscillatory rotation.

The main contributions of this paper are as follows:

- *Dynamic models*: We consider the oscillatory behavior of a vehicle undergoing off-road nav-

igation. A kinetic law for oscillatory rotation is derived. Its performance is studied both analytically and quantitatively.

- *Selective stabilization*: We investigate the separability of smooth rotation and oscillatory rotation. Selective removal of oscillatory rotation from total rotation is justified.
- *Maneuver detection*: Visual cues are exploited to instantaneously or conservatively detect the occurrence and disappearance of smooth rotation.
- *Structure from selective stabilization*: The relative positions of scene points are estimated in a stabilized frame of reference. Impressions of steering and climbing are preserved.

The organization of this paper is as follows. Section 2 discusses the observability of total rotation from visual cues. The separability of smooth rotation and oscillatory rotation, based on appropriate dynamic laws, is addressed in Section 3. The complete algorithm, including the detection of the occurrence and disappearance of smooth rotation as well as estimation of structure parameters, is presented in Section 4. Section 5 reports results of experiments using synthetic data. Conclusions are given in Section 6.

2 Observability of Full Rotation

This section addresses the observability of parameters which account for the attitude change of the vehicle carrying the camera [20]. In particular, we address parameter recovery from points and horizon lines in an image sequence. Consider a scenario in which a rigidly mounted camera undergoes rotation with instantaneous angular velocity $\omega : (\omega_x, \omega_y, \omega_z)^T$, and translation with linear velocity $\mathbf{V} : (V_x, V_y, V_z)^T$. Let $\mathbf{P} : (X, Y, Z)^T$ denote the 3-D position of a scene point with respect to the camera, and $\mathbf{p} : (x, y)^T$ the image plane coordinates of the corresponding projection point. The relative motion of the scene point with respect to the camera is then described by

$$\dot{\mathbf{P}} = -\omega \times \mathbf{P} - \mathbf{V} \quad (1)$$

Assuming that perspective projection is used as an imaging model, \mathbf{p} is related to \mathbf{P} as follows:

$$\mathbf{p} = \mathcal{P}(\mathbf{P}) + \mathbf{p}_c \quad (2)$$

where \mathbf{p}_c is the intersection of the optical axis with the image plane and \mathcal{P} denotes the perspective projection operator, i.e.

$$\mathcal{P}(\mathbf{P}) = \begin{bmatrix} f_c \frac{X}{Z} \\ f_c \frac{Y}{Z} \end{bmatrix} \quad (3)$$

with f_c the focal length. Consequently, the image motion arising from the camera movement satisfies

$$\dot{\mathbf{p}} = \underbrace{[f_c^{-1}(\mathbf{p} - \mathbf{p}_c)\omega_{xy}^{\perp T}(\mathbf{p} - \mathbf{p}_c) + \boldsymbol{\Omega}_z(\mathbf{p} - \mathbf{p}_c) + f_c\omega_{xy}^{\perp}]}_{\dot{\mathbf{p}}_r} + \underbrace{[(\mathbf{p} - \mathbf{p}_{foe})\frac{1}{\tau}]}_{\dot{\mathbf{p}}_t} \quad (4)$$

where $\mathbf{p}_{foe} = \mathcal{P}(\mathbf{V}) + \mathbf{p}_c$ and $\tau = Z/V_z$ respectively correspond to the Focus of Expansion (FOE) and the time to collision to the imaged point; $\boldsymbol{\Omega}_z$ is the 2×2 skewed symmetric matrix related to the rotational velocity component along the optical axis

$$\boldsymbol{\Omega}_z = \begin{bmatrix} 0 & \omega_z \\ -\omega_z & 0 \end{bmatrix}; \quad (5)$$

and ω_{xy}^{\perp} is an image vector orthogonal to the projection of the instantaneous angular velocity component parallel to the image plane,

$$\omega_{xy}^{\perp} = \begin{bmatrix} -\omega_y \\ \omega_x \end{bmatrix}. \quad (6)$$

Consider a distant point (i.e. let $\tau \rightarrow \infty$); denote its position by \mathbf{P} . As seen from (4) such points move relative to the camera as if only rotation were present. Therefore we may assume for these points that the 3-D motion satisfies

$$\dot{\mathbf{P}} = -\boldsymbol{\omega} \times \mathbf{P} \quad (7)$$

For off-road vehicle navigation, or images taken from an airplane or a helicopter, horizon lines or partial profiles of distant objects constitute very strong visual cues. In Figure 1, consider an image horizon line denoted by \mathcal{L} ; \mathcal{L} is uniquely characterized by \mathbf{W} , the 3-D vector normal to the plane Π through \mathcal{L} and the camera center. Since the image motion of horizon lines is explained exclusively in terms of the camera rotation, it follows that the motion of the normal vector \mathbf{W} is itself described by

$$\dot{\mathbf{W}} = -\boldsymbol{\omega} \times \mathbf{W} \quad (8)$$

If \mathbf{u} is one solution, i.e. $\dot{\mathbf{W}} = -\mathbf{u} \times \mathbf{W}$, then $k\mathbf{W} + \mathbf{u}$ also satisfies (8) for any k . Therefore, observing the image motion of one horizon line characterizes the rotational component on plane

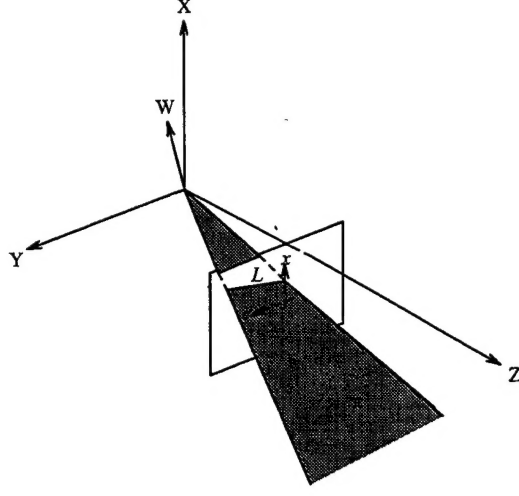


Figure 1: Geometric representation of a horizon line \mathcal{L} , the plane Π , and the 3-D normal vector \mathbf{W} .

Π only. There is indeterminacy along the direction \mathbf{W} . Given one observation, the set of possible solutions of (8) describes an affine line in 3-D rotational parameter space. Indeterminacy also exists if only one distant point is observed. In this case, this indeterminacy involves the rotational component along a ray from the image center to the point.

Quantitatively, however, lines and points carry equal amounts of information in the determination of rotation. If any combination of two of these features is observed, rotation can be fully characterized, except in some degenerate cases for which $\mathbf{W} \times \mathbf{P} = \mathbf{0}$, which in practice cannot occur unless the observer possesses an unreasonably large Field of View (FOV). Letting $\mathbf{w} = \mathcal{P}(\mathbf{W}) + \mathbf{p}_c$, one may solve the over-determined linear system

$$\mathbf{Q}\boldsymbol{\omega} = \mathbf{D} \quad (9)$$

where $\mathbf{D} = [\dot{\mathbf{p}}_1^T, \dots, \dot{\mathbf{p}}_M^T, \dot{\mathbf{w}}_1^T, \dots, \dot{\mathbf{w}}_N^T]^T$, while \mathbf{Q} is a matrix derived from (4). Line features can therefore be combined with other tracked tokens such as distant points for the recovery of rotational parameters.

When the image sequence is dense and the inter-frame motion is small, (4) effectively describes the image motion. However, irrespective of the particular trajectories of the vectors $\boldsymbol{\omega}(t)$ and $\mathbf{V}(t)$, the positions of 3-D points at two time instants can always be described by an element of the Special Euclidean group $SE(3)$ (uniquely, if the rotation center is given), i.e., there exists a total rotation $\mathbf{R} : [r_{ij}], i = 1, \dots, 3, j = 1, \dots, 3$ and translation $\mathbf{T} : (T_x, T_y, T_z)^T$, between any two frames, such

that the 3-D point positions \mathbf{P}_1 and \mathbf{P}_2 expressed in the camera frame of reference satisfy

$$\mathbf{P}_2 = \mathbf{R}\mathbf{P}_1 + \mathbf{T} \quad (10)$$

As before, for a distant point, the contribution from the translation \mathbf{T} is negligible. The image plane positions of such a point at t_1 and t_2 are then expressed as

$$\mathbf{p}_2 = (\mathbf{c}^T \mathbf{p}_1 + 1)^{-1} (\mathbf{A} \mathbf{p}_1 + \mathbf{b}) \quad (11)$$

where

$$\mathbf{A} = d^{-1} \begin{bmatrix} f_c r_{11} + x_c r_{31} & f_c r_{12} + x_c r_{32} \\ f_c r_{21} + y_c r_{31} & f_c r_{22} + y_c r_{32} \end{bmatrix} = \begin{bmatrix} a_{11} & a_{12} \\ a_{21} & a_{22} \end{bmatrix} \quad (12)$$

$$\mathbf{b} = d^{-1} \begin{bmatrix} -f_c x_c r_{11} - f_c y_c r_{12} + f_c^2 r_{13} - x_c^2 r_{31} - x_c y_c r_{32} + f_c x_c r_{33} \\ -f_c x_c r_{21} - f_c y_c r_{22} + f_c^2 r_{23} - x_c y_c r_{31} - y_c^2 r_{32} + f_c y_c r_{33} \end{bmatrix} = \begin{bmatrix} b_1 \\ b_2 \end{bmatrix} \quad (13)$$

$$\mathbf{c} = d^{-1} \begin{bmatrix} r_{31} \\ r_{32} \end{bmatrix} = \begin{bmatrix} c_1 \\ c_2 \end{bmatrix} \quad (14)$$

$$d = -x_c r_{31} - y_c r_{32} + f_c r_{33} \quad (15)$$

Similarly, for a distant line feature characterized by the projected normal vector \mathbf{w} ,

$$\mathbf{w}_2 = (\mathbf{c}^T \mathbf{w}_1 + 1)^{-1} (\mathbf{A} \mathbf{w}_1 + \mathbf{b}) \quad (16)$$

As seen from (11) and (16), for distant features, their image plane motions are described by projective group operations. This is expected since points on the horizon fall into a plane at infinity and the image motion of a plane is described exactly by a projectivity [1].

In summary, by observing the image motions of distant features, the attitude change between two frames can be estimated. Equivalently, we know the total rotation arising from steering and climbing, as well as pitch and roll, of a vehicle.

3 Selective Stabilization

The next issue concerns the separation of smooth rotation and high frequency oscillatory rotation. This procedure is important in many applications, and is referred to here as *selective stabilization*.¹ For an active vision system, the separation of oscillatory rotation from smooth rotation is useful for

¹Note that we use the term *selective stabilization* in a different sense than [3].

achieving fixation. Another example where selective stabilization is important is teleoperation, in which the vehicle needs to be remotely controlled. Information such as the 3-D locations of scene points or the knowledge of the vehicle's movement, unperturbed by the oscillatory rotation, while still preserving smooth rotation, is highly desirable; the teleoperator needs to evaluate the effects of climbing and steering. In addition, while an approximate selective stabilization scheme could be attempted by simple low-pass filtering of the computed total rotational components, a scheme which closely resembles mechanical stabilization is of greater interest.

As discussed earlier, the temporal information present in the sequence should be exploited. In addition, suitable dynamic laws also facilitate selective stabilization.

For convenience, denote the angular velocities arising from the smooth rotation the oscillatory rotation by ω_s and ω_{us} , respectively. Consider ω_s first. Since the smooth rotation is due to steering and climbing, it is assumed that the resulting attitude changes smoothly over time. A simple kinematic law is therefore employed to describe the behavior of ω_s : $(\omega_{sx}, \omega_{sy}, \omega_{sz})^T$,

$$\dot{\omega}_s = \mathbf{0} \quad (17)$$

On the other hand, the interactions between mechanical elements and the environment result in undesired oscillatory rotation. We employ a four-wheel vehicle model to account for oscillatory vehicular movement. This model takes into account the phenomena of bounce, pitch and roll (illustrated in Figure 2), and has been widely used for the design and analysis of suspension systems. Tires are modeled by linear springs with the same stiffness coefficient K_T . M_{wf} and M_{wr} represent the masses of unsprung elements such as the front and rear wheels and their axles. K_f, C_f, K_r and C_r are the characteristics of the linear springs and shock absorbers modeling the suspension system. Assuming that each tire contacts the terrain at all times, there exist seven degrees of freedom: the movements of unsprung elements $\{x_1, x_3, x_5, x_7\}$ (shown in Figure 2), the bouncing displacement of the center of gravity of the sprung element x_c , the pitch angle θ and the roll angle ϕ (illustrated in Figure 3, in which W_A and W_B constitute the wheel base, while $T_{s,r}$ and $T_{s,l}$ are the suspension tracks). Their behavior is described in detail in Appendix A. Consequently, if we define \mathbf{x}_{us} to be the vector containing the unstabilized rotational components,

$$\mathbf{x}_{us} \stackrel{\text{def}}{=} (\theta, \dot{\theta}, \phi, \dot{\phi})^T \quad (18)$$

then \mathbf{x}_{us} satisfies

$$\dot{\mathbf{x}}_{us} = \Phi_{us} \mathbf{x}_{us} + \Gamma_{us} \mathbf{u}_{us} \quad (19)$$

where \mathbf{u}_{us} includes other dependent quantities,

$$\mathbf{u}_{us} \stackrel{\text{def}}{=} (\mathbf{x}_b^T, \mathbf{x}_w^T)^T \quad (20)$$

with $\mathbf{x}_b = (x_c, \dot{x}_c)^T$ and $\mathbf{x}_w = (x_1, \dot{x}_1, x_3, \dot{x}_3, x_5, \dot{x}_5, x_7, \dot{x}_7)^T$. Φ_{us} and Γ_{us} respectively denote constant matrices whose entries are related to system parameters such as the mass of the sprung element, the moment of inertia, the spring characteristics, etc. Since additional sensors such as accelerometers are required for obtaining \mathbf{u}_{us} , we instead approximate the behavior of \mathbf{x}_{us} by

$$\dot{\mathbf{x}}_{us} = \Phi_{us} \mathbf{x}_{us} \quad (21)$$

It is shown in Appendix B that this approximation introduces an additional error in separating smooth rotation and oscillatory rotation. However, the error remains bounded.

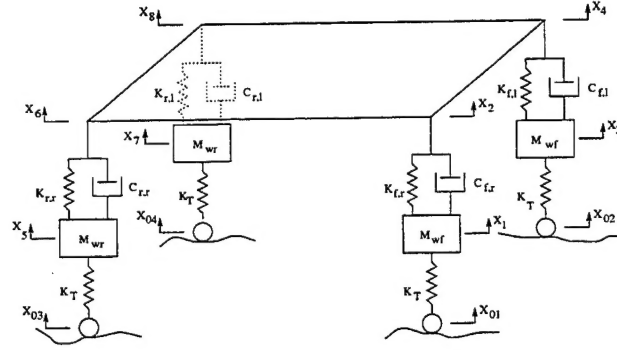


Figure 2: The four-wheel vehicle model [7]: $\{x_{0i}, i = 1, \dots, 4\}$ denotes the disturbances from the terrain; $\{x_1, x_3, x_5, x_7\}$ represent the displacements of the unsprung elements; and $\{x_2, x_4, x_6, x_8\}$ are the movements of the four corners to which the suspension system is connected.

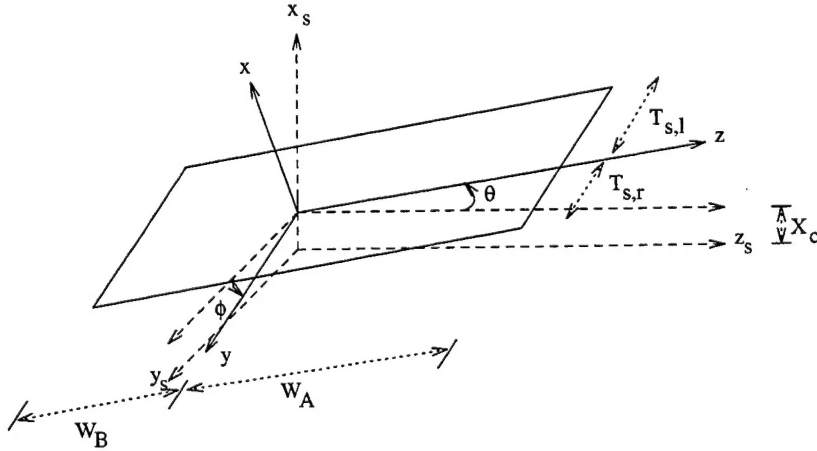


Figure 3: The relationship between the stabilized coordinate system \mathcal{V}_s and the oscillatory coordinate system \mathcal{V} ; the bounce x_c , the pitch angle θ , and the roll angle ϕ .

We now address the separation of smooth rotation and oscillatory rotation using the dynamic law in (21). Consider Figure 3. Define the stabilized coordinate system $\mathcal{V}_s(t)$ whose orientation is determined by the smooth rotation, and whose center is located at the center of gravity of the vehicle. Consider also the unstabilized coordinate system $\mathcal{V}(t)$, whose attitude is in addition affected by the oscillatory rotation, and with its origin shifted from the center of gravity due to bounce. Then, as argued in the previous section, from two images acquired at times $t - \Delta t$ and t , we observe the total angular velocity accounting for the net attitude change between $\mathcal{V}(t - \Delta t)$ and $\mathcal{V}(t)$. In other words, if $\mathbf{R}(\omega; t, t - \Delta t)$ aligns the coordinate system $\mathcal{V}(t - \Delta t)$ with $\mathcal{V}(t)$, $\mathbf{R}_s(\omega_s; t, t - \Delta t)$ takes into account the attitude difference between $\mathcal{V}_s(t - \Delta t)$ and $\mathcal{V}_s(t)$, and $\mathbf{R}_{us}(\theta, \phi; t)$ accounts for the additional attitude due to the oscillatory rotation at time t ,

$$\mathbf{R}_{us}(\theta, \phi; t) = \begin{bmatrix} 1 & \phi(t) & -\theta(t) \\ -\phi(t) & 1 & 0 \\ \theta(t) & 0 & 1 \end{bmatrix} \quad (22)$$

then it can be shown that

$$\mathbf{R}(\omega; t, t - \Delta t) = \mathbf{R}_{us}(\theta, \phi; t) \mathbf{R}_s(\omega_s; t, t - \Delta t) \mathbf{R}_{us}^{-1}(\theta, \phi; t - \Delta t) \quad (23)$$

Subsequently, assume that \mathbf{R} and \mathbf{R}_s can be approximated as

$$\mathbf{R}(\omega; t, t - \Delta t) \approx \mathbf{I} - \boldsymbol{\Omega} \Delta t \quad (24)$$

$$\mathbf{R}_s(\omega_s; t, t - \Delta t) \approx \mathbf{I} - \boldsymbol{\Omega}_s \Delta t \quad (25)$$

with

$$\boldsymbol{\Omega} = \begin{bmatrix} 0 & -\omega_z & \omega_y \\ \omega_z & 0 & -\omega_x \\ -\omega_y & \omega_x & 0 \end{bmatrix} \quad \text{and} \quad \boldsymbol{\Omega}_s = \begin{bmatrix} 0 & -\omega_{sz} & \omega_{sy} \\ \omega_{sz} & 0 & -\omega_{sx} \\ -\omega_{sy} & \omega_{sx} & 0 \end{bmatrix} \quad (26)$$

Also,

$$\begin{aligned} \frac{\theta(t) - \theta(t - \Delta t)}{\Delta t} &\approx \dot{\theta}(t) \\ \frac{\phi(t) - \phi(t - \Delta t)}{\Delta t} &\approx \dot{\phi}(t) \end{aligned} \quad (27)$$

Then the total angular velocity ω is related to the angular velocity due to the smooth rotation and oscillatory rotation by

$$\omega = \omega_s + \omega_{us} \quad (28)$$

with

$$\omega_{us} \stackrel{\text{def}}{=} (0, \dot{\theta}, \dot{\phi})^T \quad (29)$$

Since the angular velocity component due to the yaw motion is assumed to be zero, we only focus on the separability of the other two phenomena, i.e. climbing and pitch as well as banking and roll. Using the dynamic laws in (17) and (21), the following linear system can be constructed:

$$\begin{cases} \dot{\mathbf{x}}_1 = \mathbf{G}\mathbf{x}_1 \\ \boldsymbol{\omega}_1 = \mathbf{F}\mathbf{x}_1 \end{cases} \quad (30)$$

where $\mathbf{x}_1 = (\omega_{sy}, \omega_{sz}, \mathbf{x}_{us}^T)^T$, $\boldsymbol{\omega}_1 = (\omega_y, \omega_z)^T$,

$$\mathbf{G} = \begin{bmatrix} \mathbf{0}_{2 \times 2} & \mathbf{0}_{2 \times 4} \\ \mathbf{0}_{4 \times 2} & \boldsymbol{\Phi}_{us} \end{bmatrix} \quad (31)$$

with $\mathbf{0}_{2 \times 2}$, $\mathbf{0}_{2 \times 4}$ and $\mathbf{0}_{4 \times 2}$ being zero matrices of conformable dimensions,

$$\mathbf{F} = \begin{bmatrix} 1 & 0 & 0 & 1 & 0 & 0 \\ 0 & 1 & 0 & 0 & 0 & 1 \end{bmatrix} \quad (32)$$

The separability of smooth rotation and oscillatory rotation can now be verified by checking the rank of the observability matrix \mathbf{O} ,

$$\mathbf{O} = \begin{bmatrix} \mathbf{F} \\ \mathbf{F}\mathbf{G} \\ \vdots \\ \mathbf{F}\mathbf{G}^5 \end{bmatrix} \quad (33)$$

Except in some special cases in which the matrix $\boldsymbol{\Phi}_{us}$ is singular, \mathbf{O} in general has full rank. Therefore, by employing different dynamic laws to describe the smooth rotation and oscillatory rotation, it is possible to separate the two rotation phenomena. The next section presents schemes for the estimation of total angular velocity, the detection of the occurrence and disappearance of smooth rotation, and the 3-D location of close feature points in the stabilized coordinate system.

4 Parameter Estimation

The observability of total rotation from distant features indicates that the recovery of the total angular velocity can be achieved using an LS solution in (9). However, the estimation benefits if temporal information is exploited. In addition, the incorporation of appropriate dynamic laws to describe smooth rotation and oscillatory rotation shows the possibility of selective stabilization. Nonetheless, since smooth rotation does not occur at all times, awareness of the occurrence or disappearance of smooth rotation, especially climbing, facilitates the task. This section describes various techniques which constitute our algorithm for off-road navigation.

4.1 Image Stabilization

Because of the desirable properties of recursive estimators, we employ an Extended Kalman Filter (EKF) to estimate the total angular velocity ω [20]. The state vector \mathbf{x} is defined as

$$\mathbf{x} \stackrel{\text{def}}{=} \omega \quad (34)$$

To exploit temporal information for robust estimation, a simple kinematic law is used:

$$\dot{\mathbf{x}} = \mathbf{0} \quad (35)$$

Subsequently,

$$\mathbf{x}(t_{i+1}) = \mathbf{x}(t_i) \quad (36)$$

This constitutes the plant equation in our recursive estimation algorithm. We turn next to the observation equations. Assume that the tracked tokens consist of M points (whose projection points are $\mathbf{p}_1, \dots, \mathbf{p}_M$) and N horizon lines (each with associated normal vector $\mathbf{w}_i, i = 1, \dots, N$). The measurement vector is defined by

$$\mathbf{z} = (\mathbf{p}_1^T, \dots, \mathbf{p}_M^T, \mathbf{w}_1^T, \dots, \mathbf{w}_N^T)^T \quad (37)$$

Then, from (11) and (16), we obtain the measurement equations as

$$\mathbf{z}(t_{i+1}) = \mathbf{h}_{i+1,i}[\mathbf{x}(t_{i+1})] + \mathbf{n}(t_{i+1}) \quad (38)$$

where \mathbf{h} is a nonlinear function while \mathbf{n} denotes the measurement noise. More specifically, $\mathbf{h}_{i+1,i}[\mathbf{x}(t_{i+1})]$ is expressed as

$$\mathbf{h}_{i+1,i}[\mathbf{x}(t_{i+1})] = \begin{bmatrix} (\mathbf{c}^T \mathbf{p}_1 + 1)^{-1}(\mathbf{A} \mathbf{p}_1 + \mathbf{b}) \\ \vdots \\ (\mathbf{c}^T \mathbf{p}_M + 1)^{-1}(\mathbf{A} \mathbf{p}_M + \mathbf{b}) \\ (\mathbf{c}^T \mathbf{w}_1 + 1)^{-1}(\mathbf{A} \mathbf{w}_1 + \mathbf{b}) \\ \vdots \\ (\mathbf{c}^T \mathbf{w}_N + 1)^{-1}(\mathbf{A} \mathbf{w}_N + \mathbf{b}) \end{bmatrix} \quad (39)$$

with $\mathbf{A}, \mathbf{b}, \mathbf{c}$ defined in (12)–(15).

After the horizon lines and points are tracked, the EKF scheme is applied to estimate the total angular velocity. This consists of the following steps:

- **Step 1:** State and covariance propagation:

$$\begin{aligned}\hat{\mathbf{x}}(t_{i+1}^-) &= \hat{\mathbf{x}}(t_i^+) \\ \Sigma(t_{i+1}^-) &= \Sigma(t_i^+) + \Sigma_w(t_{i+1})\end{aligned}\tag{40}$$

where $\hat{\mathbf{x}}(t_i^+)$ and $\Sigma(t_i^+)$ denote the estimates of $\mathbf{x}(t_i)$ and the associated covariances: they are obtained based on information contained in the sequence up to the i^{th} frame. $\hat{\mathbf{x}}(t_{i+1}^-)$ and $\Sigma(t_{i+1}^-)$, on the other hand, are the predicted estimates of $\mathbf{x}(t_{i+1})$ and the predicted covariances, respectively, before the incorporation of the $(i+1)^{\text{th}}$ frame, while $\Sigma_w(t_{i+1})$ is the covariance of the plant noise $\mathbf{w}(t_{i+1})$.

- **Step 2:** State and covariance update:

$$\begin{aligned}\mathbf{K}(t_{i+1}) &= \Sigma(t_{i+1}^-) \mathbf{H}_{i+1,i}^T [\mathbf{H}_{i+1,i} \Sigma(t_{i+1}^-) \mathbf{H}_{i+1,i}^T + \Sigma_n(t_{i+1})]^{-1} \\ \hat{\mathbf{x}}(t_{i+1}^+) &= \hat{\mathbf{x}}(t_{i+1}^-) + \mathbf{K}(t_{i+1}) \{ \mathbf{z}(t_{i+1}) - \mathbf{h}_{i+1,i}[\hat{\mathbf{x}}(t_{i+1}^-)] \} \\ \Sigma(t_{i+1}^+) &= [\mathbf{I} - \mathbf{K}(t_{i+1}) \mathbf{H}_{i+1,i}] \Sigma(t_{i+1}^-)\end{aligned}\tag{41}$$

where $\hat{\mathbf{x}}(t_{i+1}^+)$ is the desired estimate of $\mathbf{x}(t_{i+1})$, and $\Sigma(t_{i+1}^+)$ is the associated covariance. $\mathbf{K}(t_{i+1})$, $\Sigma_n(t_{i+1})$ and \mathbf{I} respectively represent the gain matrix, the covariance of $\mathbf{n}(t_{i+1})$, and the identity matrix. $\mathbf{H}_{i+1,i}$, on the other hand, is the linearized approximation of $\mathbf{h}_{i+1,i}$,

$$\mathbf{H}_{i+1,i} = \left. \frac{\partial \mathbf{h}_{i+1,i}}{\partial \mathbf{x}(\mathbf{t}_{i+1})} \right|_{\hat{\mathbf{x}}(t_{i+1}^-)}\tag{42}$$

With the above formulation, we now proceed to describe the detection scheme which facilitates selective stabilization.

4.2 Separation of Smooth Rotation and Oscillatory Rotation

As discussed earlier, when the high frequency yaw motion is negligible, steering is directly known from the total angular velocity. Similarly, the phenomenon of banking only lasts for short periods, and more importantly, it has no effect on the direction in which the vehicle travels later. Banking is therefore also neglected. Consequently, the roll motion is obtained directly. On the other hand, climbing is not negligible; the vehicle generally moves along a direction resulting from climbing. Thus, the separation of climbing and pitch motions is important. Like the other types of smooth rotation, climbing only lasts for short periods. Therefore, we design a scheme to detect the occurrence and disappearance of climbing. The detection results are then used to adjust the selective stabilization scheme.

Recall the image motion expressed in (4). When a distant point is considered, its vertical movement is described by

$$\dot{x} = \omega_x[(x - x_c)(y - y_c)] - \omega_y[f_c + (x - x_c)^2] + \omega_z(y - y_c) \quad (43)$$

If the corresponding projection point is close to the vertical axis, i.e. $y - y_c \approx 0$, then

$$\dot{x} \approx -\omega_y[f_c + (x - x_c)^2] \quad (44)$$

In other words, the vertical movements of such features are dominantly affected by climbing and pitch motions. Since the previously designed scheme assumes a zero order dynamic law for the total angular velocity, it is expected that when the vehicle performs maneuvers (i.e. starts climbing or finishes climbing), there appear *large* errors in predicting the vertical movements of corresponding points at these instants. Consequently, we define $[\mathbf{z}_m]_x$ to be the vector consisting of the vertical coordinates of N such feature points, $\mathbf{p}_{m1}, \dots, \mathbf{p}_{mN}$, i.e.

$$[\mathbf{z}_m]_x = ([\mathbf{p}_{m1}]_x, \dots, [\mathbf{p}_{mN}]_x)^T \quad (45)$$

and the test statistic δ at time t as

$$\delta(t) \stackrel{\text{def}}{=} ([\mathbf{z}_m(t)]_x - [\hat{\mathbf{z}}_m(t)]_x)^T \Sigma_m^{-1}(t) ([\mathbf{z}_m(t)]_x - [\hat{\mathbf{z}}_m(t)]_x) \quad (46)$$

where $\hat{\mathbf{z}}_m(t)$ denotes the predicted locations of these N feature points at time t ; it is computed according to (11), in which the projections of the 3-D points at $t - \Delta t$ are used as \mathbf{p}_1 , while the predicted value of total angular velocity is assumed in obtaining $\mathbf{A}, \mathbf{b}, \mathbf{c}$. $\Sigma_m(t)$, on the other hand, is the covariance matrix of the innovation vector $[\mathbf{z}_m(t)]_x - [\hat{\mathbf{z}}_m(t)]_x$; it can easily be computed in our EKF formulation. Based on $\delta(t)$, we declare that the vehicle undergoes maneuvers at $t - \Delta t$ when

$$\delta(t) > TH \quad (47)$$

with TH a threshold value. The types of maneuvers corresponding to the occurrence or disappearance of climbing can then be determined. If the vehicle undergoes climbing at a rate $\omega_{sy}(t)$ much larger than the pitching velocity $\dot{\theta}(t)$, the resulting maneuver can be identified by comparing $\delta(t)$ to previous non-maneuver test statistics $\delta(t - \Delta t), \delta(t - 2\Delta t), \dots, \delta(t - m\Delta t)$, with m the size of a moving window. Similarly, if the type of maneuver leads to the disappearance of ω_{sy} in ω_y , the scheme also reacts instantaneously.

There are situations in which the attitude change due to climbing, at maneuver instants, is less than the change arising from pitch motion. On these occasions, if we regard $\omega_{sy}(t)$ as the desired signal, and $\dot{\theta}(t)$ as the additive noise, we are dealing with a problem involving a small signal to noise ratio. The test statistic $\delta(t)$ may become inappropriate since the maneuver test statistic does not manifest itself in larger values. We therefore impose another conservative criterion. This criterion cannot detect maneuvers instantaneously. However, it notices the event a few frames later and prevents the divergence of the algorithm.

Specifically, observe that when the vehicle only undergoes pitch motion, $\mathbf{p}_{m1}, \dots, \mathbf{p}_{mN}$ are likely to oscillate around their own reference positions. The conservative detection criterion monitors the vertical movements of these points with some frequency less than the sequence acquisition rate. If these N points move away from the reference positions, the algorithm reports the occurrence of climbing. Reprocessing a small set of images is then performed. Similarly, when the smooth climbing ends, these points oscillate around new reference positions. Appropriate actions are then taken.

We now proceed to address the separation of climbing and pitch motions. When the occurrence of climbing is detected, the algorithm responds by incorporating different dynamic laws for selective stabilization. When the scheme detects the disappearance of climbing, the algorithm concentrates on obtaining the relevant information of the pitch angle θ using the estimated ω_y . Let the vector \mathbf{y} consist of the quantities of interest. When there is only pitch motion,

$$\mathbf{y} = (\theta, \dot{\theta})^T; \quad (48)$$

otherwise, \mathbf{y} is augmented to include the climbing component:

$$\mathbf{y} = (\omega_{sy}, \theta, \dot{\theta})^T \quad (49)$$

Then, as discussed in Section 3, by using the dynamic laws in (17) and (21), climbing and pitch motion can be separated. To take into account the noise in the estimate of ω_y , we apply another Kalman Filter to estimate \mathbf{y} . Using the assumptions that

$$\begin{aligned} \omega_{sx} &= \omega_x \\ \dot{\phi} &= \omega_z \end{aligned} \quad (50)$$

we have therefore separated the smooth rotation and oscillatory rotation. The next section discusses the use of selective stabilization to recover the 3-D locations of feature points which are close to the vehicle.

4.3 Structure from Selective Stabilization

Recall that the motion of a close 3-D point relative to the stabilized coordinate system \mathcal{V}_s is described by

$$\dot{\mathbf{P}}_{\mathcal{V}_s} = -\boldsymbol{\omega}_s \times \mathbf{P}_{\mathcal{V}_s} - \mathbf{V}_s \quad (51)$$

where $\mathbf{P}_{\mathcal{V}_s}$ denotes the coordinates of the point in \mathcal{V}_s , $\boldsymbol{\omega}_s$ is the angular velocity due to the smooth rotation, and \mathbf{V}_s is the vehicle's translational velocity under no disturbances. When the vehicle undergoes constant smooth rotation and translation between $t - \Delta t$ and t , we have

$$\mathbf{P}_{\mathcal{V}_s}(t) = \mathbf{R}_s(\boldsymbol{\omega}_s; t, t - \Delta t) \mathbf{P}_{\mathcal{V}_s}(t - \Delta t) + \mathbf{T}_s(\boldsymbol{\omega}_s; t, t - \Delta t) \quad (52)$$

where \mathbf{R}_s accounts for the resulting attitude change as explained in (25), while \mathbf{T}_s can be shown [21] to be

$$\mathbf{T}_s(\boldsymbol{\omega}_s; t, t - \Delta t) = - \left[\mathbf{I} \Delta t - \frac{1 - \cos(|\boldsymbol{\omega}_s| \Delta t)}{|\boldsymbol{\omega}_s|^2} \boldsymbol{\Omega}_s + \frac{|\boldsymbol{\omega}_s| \Delta t - \sin(|\boldsymbol{\omega}_s| \Delta t)}{|\boldsymbol{\omega}_s|^3} \boldsymbol{\Omega}_s^2 \right] \mathbf{V}_s \quad (53)$$

with $\boldsymbol{\Omega}_s$ being defined in (26) and $|\boldsymbol{\omega}_s|$ denoting the magnitude of $\boldsymbol{\omega}_s$. In particular, observing that the translational movement of a vehicle is along its longitudinal axis most of the time [12], \mathbf{V}_s is simplified to

$$\mathbf{V}_s = (0, 0, v_s)^T \quad (54)$$

with v_s being the forward speed. Since v_s can easily be obtained from the odometer, we assume that it is known. \mathbf{T}_s is then simplified accordingly.

The relative motion of the point with respect to the unstabilized coordinate system \mathcal{V} is then obtained as

$$\mathbf{P}_{\mathcal{V}}(t) = \mathbf{R}_{us}(\theta, \phi; t) \{ \mathbf{P}_{\mathcal{V}_s}(t) - \mathbf{T}_{us}(t) \} \quad (55)$$

where \mathbf{T}_{us} is due to the bounce of the vehicle,

$$\mathbf{T}_{us}(t) = (x_c(t), 0, 0)^T \quad (56)$$

The projection of the 3-D point on the image is then computed by applying the perspective projection operator \mathcal{P} :

$$\mathbf{p} = \mathcal{P}(\mathbf{P}_{\mathcal{V}} - \mathbf{d}) + \mathbf{p}_c \quad (57)$$

where \mathbf{d} specifies the position of the camera with respect to \mathcal{V} ; it remains constant because the camera is mounted rigidly on the vehicle. Since the effect of \mathbf{T}_{us} is usually too small to be observed

from the images, it is not considered. Therefore, by tracking the points of interest over the sequence, as well as using the estimates from selective stabilization, we again obtain a system suitable for recursive estimators such as EKF. The corresponding plant equations for M_s such points are

$$\mathbf{P}_{\nu,j}(t_{i+1}) = \mathbf{R}_s(\omega_s; t_{i+1}, t_i) \mathbf{P}_{\nu,j}(t_i) + \mathbf{T}_s(\omega_s; t_{i+1}, t_i) \quad j = 1 \cdots M_s \quad (58)$$

The measurement equations, on the other hand, are

$$\mathbf{p}_j = \mathcal{P}(\mathbf{P}_{\nu,j} - \mathbf{d}) + \mathbf{p}_c \quad j = 1 \cdots M_s \quad (59)$$

As seen from (58), close features are estimated in the stabilized frame of reference. The undesired oscillatory phenomena seen from the unstabilized coordinate system are removed.

This concludes our scheme for off-road navigation using selective stabilization. The next section presents simulation results.

5 Synthetic Experiments

In this section we illustrate the proposed approach through synthetic experiments. Two experiments were performed. One corresponds to the situation in which the attitude change due to climbing is *much* larger than the change arising from pitch motion, the so-called high signal to noise ratio case. The other one deals with the case involving low signal to noise ratio.

Consider the scenario in which the vehicle undergoes steering for the first one second, with a rate of $\omega_{sx} = 0.1 \text{ rad} \cdot \text{s}^{-1}$. Immediately after the steering, the vehicle starts climbing over a hill. The smooth rotation due to climbing exists for two seconds. The climbing rates are set to $\omega_{sy} = 0.1 \text{ rad} \cdot \text{s}^{-1}$ and $0.01 \text{ rad} \cdot \text{s}^{-1}$, in the high and low signal to noise ratio situations respectively. Finally, the vehicle moves uphill along a straight path for the last two seconds, i.e. no smooth rotation occurs. The forward speed of the vehicle is maintained at $v_s = 10.0 \text{ m} \cdot \text{s}^{-1}$.

The surface irregularities, on the other hand, are modeled using first order Markov processes; their coefficients depend on the terrain roughness and the vehicle's forward speed. Therefore, the excitations to the vehicle are given by

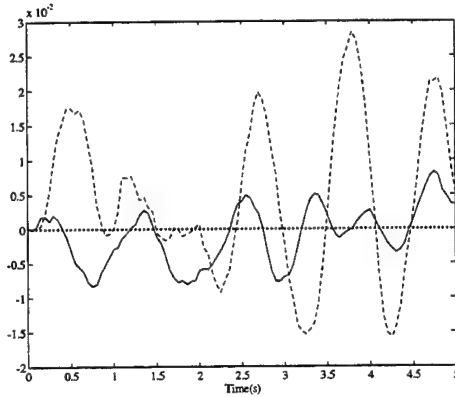
$$\dot{x}_{0i}(t) = -avx_{0i}(t) + n_{av}(t) \quad i = 1 \cdots 4 \quad (60)$$

where n_{av} is the white, Gaussian driving noise with mean zero and variance set to $2\sigma^2av$. The values of a and σ , in addition, vary for different surfaces. We choose $\sigma = 0.012 \text{ m}$ and $a = 0.8 \text{ m}^{-1}$ [15].

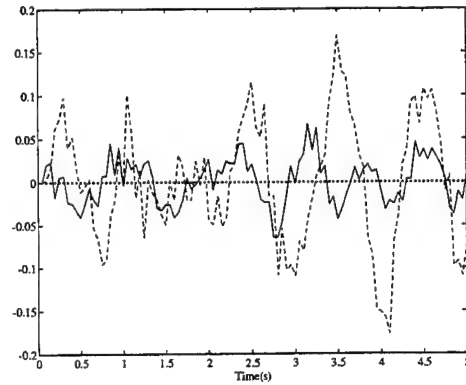
The nominal values of the vehicle's parameters are listed in Table 1. According to the equations of motion derived in Appendix A, we synthesize the oscillatory behavior of the vehicle and illustrate it in Figure 4 (only pitch and roll phenomena are shown). Together with the smooth motion, the unstabilized behavior of the vehicle is obtained.

Table 1: The nominal parameter values of the four-wheel vehicle model.

M_B	I_{yy}	I_{zz}	M_{wf}
1710.0kg	1031.3kg · m ²	201.8kg · m ²	57.5kg
M_{wr}	K_T	$C_f (C_r)$	K_f
75.0kg	200.0 kN · m ⁻¹	1.0 kN · m ⁻¹ · s ⁻¹	18.0 kN · m ⁻¹
K_r	$T_{s,r} (T_{s,l})$	W_A	W_B
10.0 kN · m ⁻¹	0.6m	1.4m	1.3m



(a)



(b)

Figure 4: An example of the pitch (solid line) and roll (dashed line) behavior of the nominal vehicle. (a) $\theta(t)$ and $\phi(t)$, (b) $\dot{\theta}(t)$ and $\dot{\phi}(t)$.

In addition, during driving, a sequence of images is acquired at 20 Hz from an on-board camera (each image has size 2.0×2.0 and resolution 2000×2000), while a set of features including eight distant points and four close points are tracked. The coordinates of these points with respect to the initial frame of reference are listed in Table 2.

The algorithm is now applied to estimate the total angular velocity, to separate the rotation due to climbing and pitch motion, as well as to obtain the 3-D locations of four close features with respect to the stabilized coordinate system.

Table 2: The initial 3-D locations of the feature points: the first eight points are regarded as distant features, while the last four are considered to be close features.

Point	3-D coordinates			Point	3-D coordinates			Point	3-D coordinates		
1	1260	36	1800	5	1620	1440	1800	9	45.5	-45.5	65.0
2	1600	-20	2000	6	1400	-1400	2000	10	46.4	-23.2	58.0
3	-1840	-69	2300	7	1150	-920	2300	11	45.0	30.0	60.0
4	-1575	70	1750	8	875	875	1750	12	42.0	56.0	70.0

5.1 High Signal to Noise Ratio

We consider here the situation in which the vehicle climbs uphill with a high climbing rate, $\omega_{sy} = 0.1 \text{ rad} \cdot \text{s}^{-1}$. The performance of the algorithm is evaluated from 50 Monte Carlo trials. The total angular velocity is first computed from eight listed distant points. The resulting x and z components are directly regarded as the steering rate ω_{sx} and the roll velocity $\dot{\phi}$. Figures 5 and 7 respectively show the corresponding bias and root mean-square errors of the two estimates. The estimate of ω_y is illustrated in Figure 6a. Meanwhile, to detect the occurrence of climbing, the test statistic δ is calculated by considering the vertical movements of points 1–4, and is shown in Figure 6b. As seen from Figure 6b, δ exhibits large values when maneuvers occur ($t = 1.0 \text{ s}$ and $t = 3.0 \text{ s}$). Thus maneuvers can be detected instantaneously. We thereupon take ω_{sy} into consideration from $t = 1.0 \text{ s}$ to $t = 3.0 \text{ s}$. The results of selective stabilization are shown in Figure 8. It can be seen that the algorithm separates climbing and pitch phenomena quite well. After selective stabilization has been achieved, these estimates are used in obtaining 3-D information about close features, i.e. points 9–12. The initial guesses about these points are listed in Table 3, while the estimates are shown in Figure 9. The respective estimates exhibit similar behaviors; therefore only the results for the 12th point are displayed. It is observed that, when the signal to noise ratio is high, the algorithm provides satisfactory estimates which should be useful for off-road navigation.

Table 3: Initial guesses of the 3-D locations of points 9–12.

Point	3-D coordinates		
9	42.3	-42.9	60.0
10	40.4	-20.5	50.0
11	37.9	25.6	50.0
12	36.2	48.9	60.0

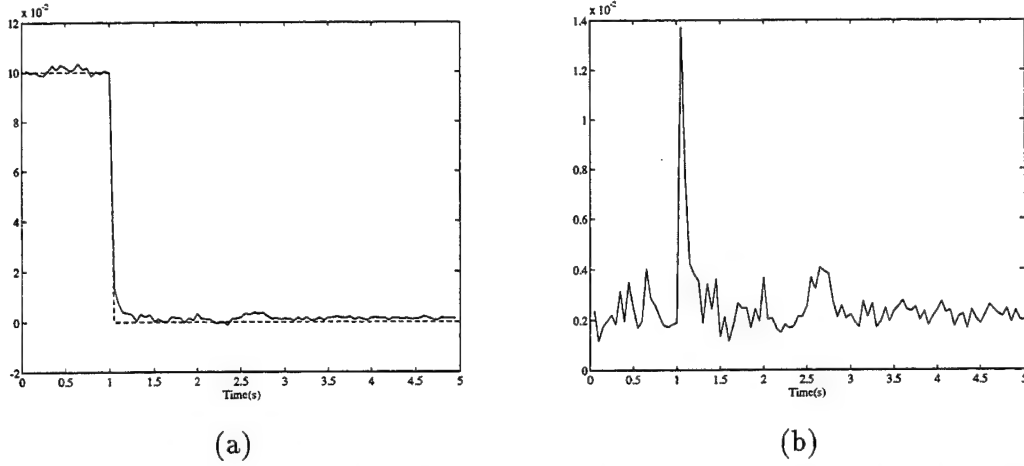


Figure 5: Estimates of the steering rate ω_{sx} , in the high signal to noise ratio case, from 50 Monte Carlo trials. (a) True (dashed line) and estimated (solid line), (b) root mean-square error.

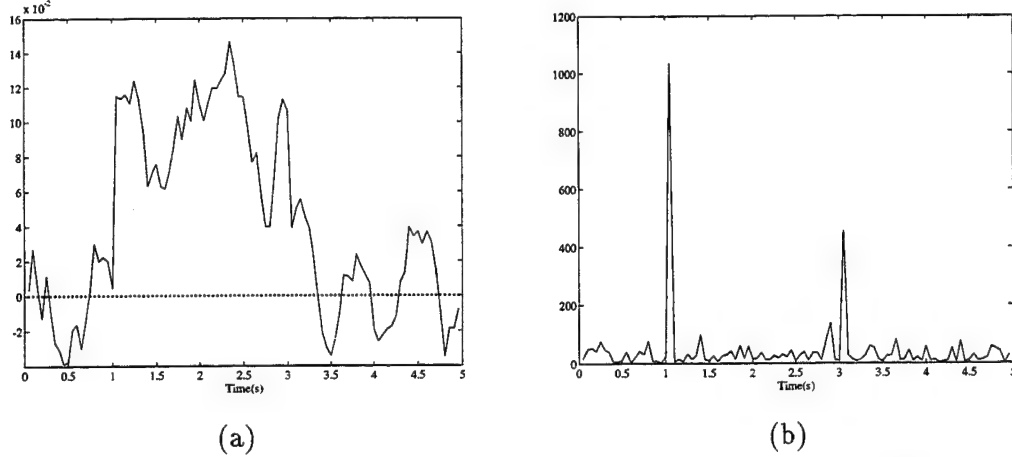


Figure 6: Estimates of the climbing-pitch rate ω_y and test statistic δ , in the high signal to noise ratio case, from 50 Monte Carlo trials. (a) ω_y , (b) δ .

5.2 Low Signal to Noise Ratio

We now present some results corresponding to the low signal to noise ratio case, i.e. the vehicle undergoes climbing at a small rate, $\omega_{sy} = 0.01 \text{ rad} \cdot \text{s}^{-1}$. Again, the performance is evaluated from 50 Monte Carlo trials. Figures 10a and 10b show the estimates of the total angular velocity ω and the test statistic δ . Since the x and z components of ω exhibit behavior similar to that in the high signal to noise ratio case, they are not displayed here. On the other hand, contrast with Figure 6b, the test statistic δ does not manifest large values at $t = 1.0$ s and $t = 3.0$ s. The occurrence and disappearance of climbing are therefore not detected instantaneously. However, by monitoring the vertical movements of the first four distant points at the rate of 2 Hz, as shown in

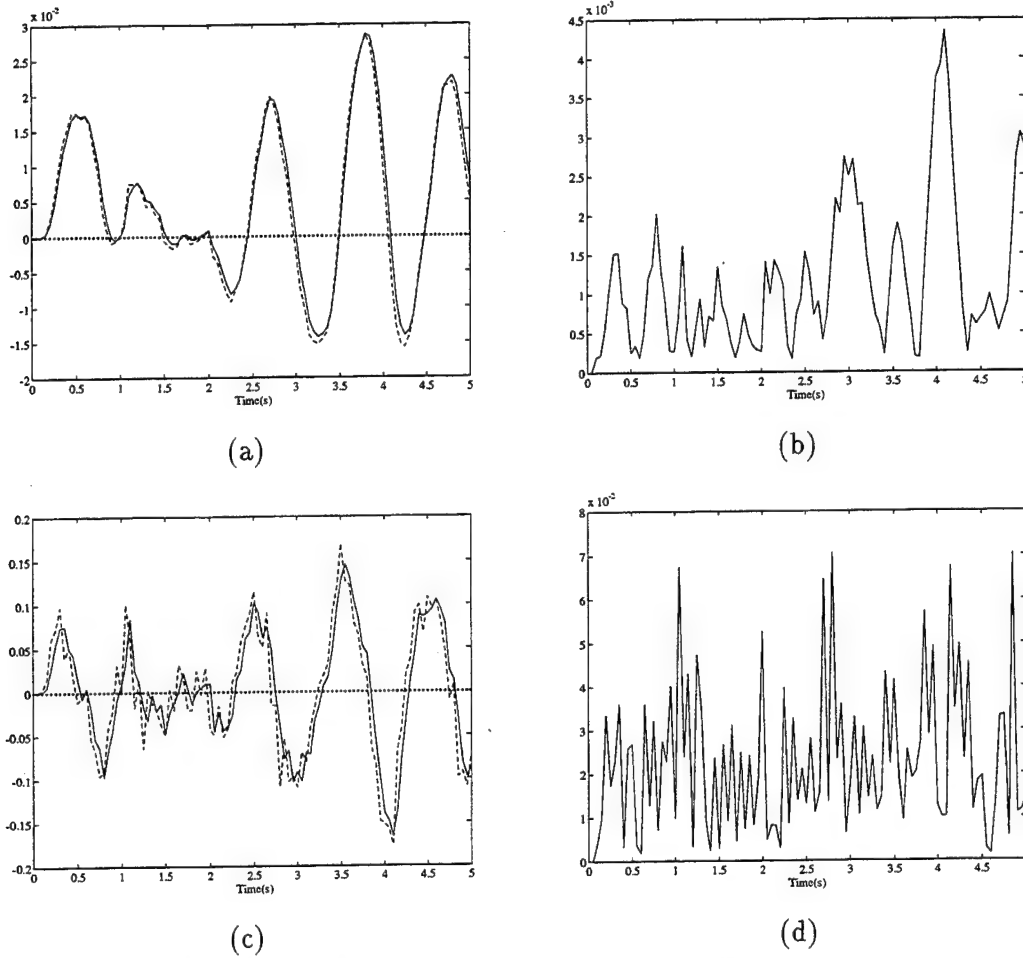
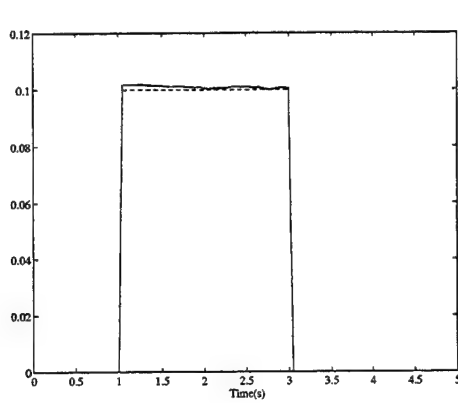
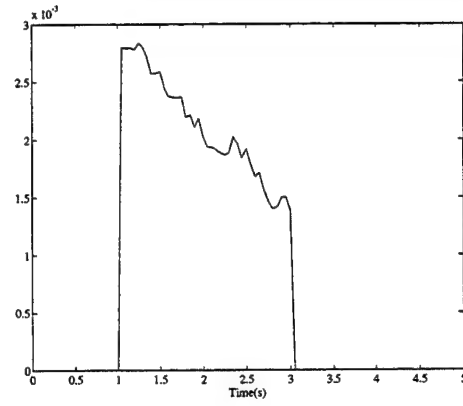


Figure 7: Estimates of roll-related parameters, in the high signal to noise ratio case, from 50 Monte Carlo trials. (a) ϕ : true (dashed line) and estimated (solid line), (b) ϕ : root mean-square error, (c) $\dot{\phi}$: true (dashed line) and estimate (solid line), (d) $\dot{\phi}$: root mean-square error.

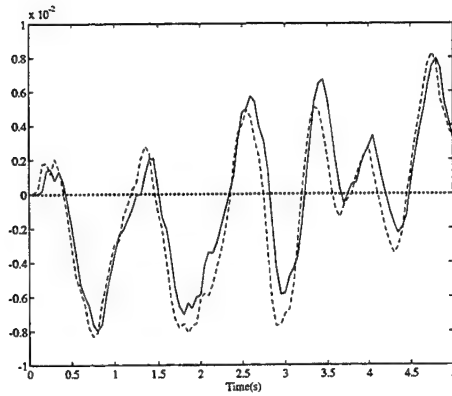
Figure 11, the scheme observes that these points move away from their first reference positions at $t = 2.5$ s. Consequently, the algorithm reprocesses the sequence from the image acquired at $t = 0.5$ s. Similarly, after $t = 3.5$ s, these points oscillate around new reference positions. The scheme declares the instant the climbing disappears to be $t = 3.5$ s. Based on these conservative decisions, the selective stabilization results are shown in Figure 13. As seen from this figure, the estimate of ω_{sy} is noisier in this case. This leads to degradation in the estimates of θ and $\dot{\theta}$. The results corresponding to the 3-D locations of close feature points are shown in Figure 12. They exhibit a slightly larger bias. This is expected since the orientation of the stabilized coordinate system \mathcal{V}_s is biased because of the additional smooth rotation that presumably occurred between $t = 3.0$ s and $t = 3.5$ s. Irrespective of these relatively larger biases, the corresponding absolute errors remain small. The structure information is therefore more or less preserved.



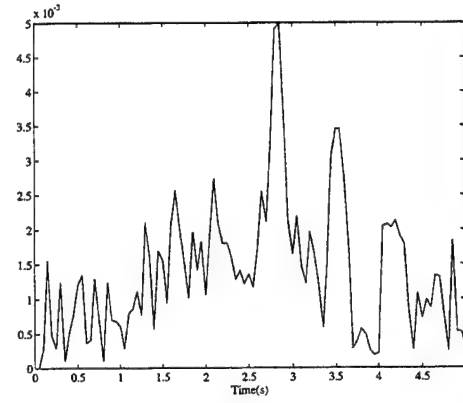
(a)



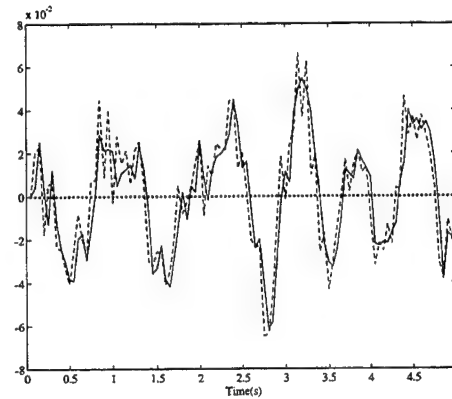
(b)



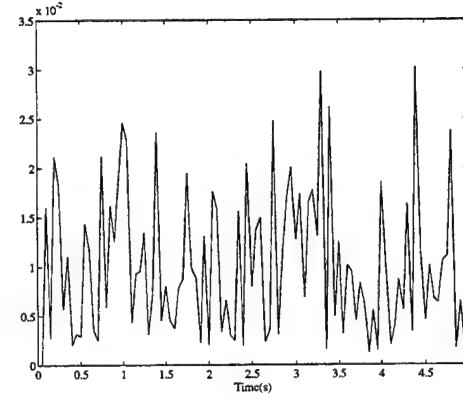
(c)



(d)



(e)



(f)

Figure 8: Estimates of climbing-pitch parameters, in the high signal to noise ratio case, from 50 Monte Carlo trials. (a) ω_{sy} : true (dashed line) and estimated (solid line), (b) ω_{sy} : root mean-square error, (c) θ : true (dashed line) and estimated (solid line), (d) θ : root mean-square error, (e) $\dot{\theta}$: true (dashed line) and estimated (solid line), (f) $\dot{\theta}$: root mean-square error.

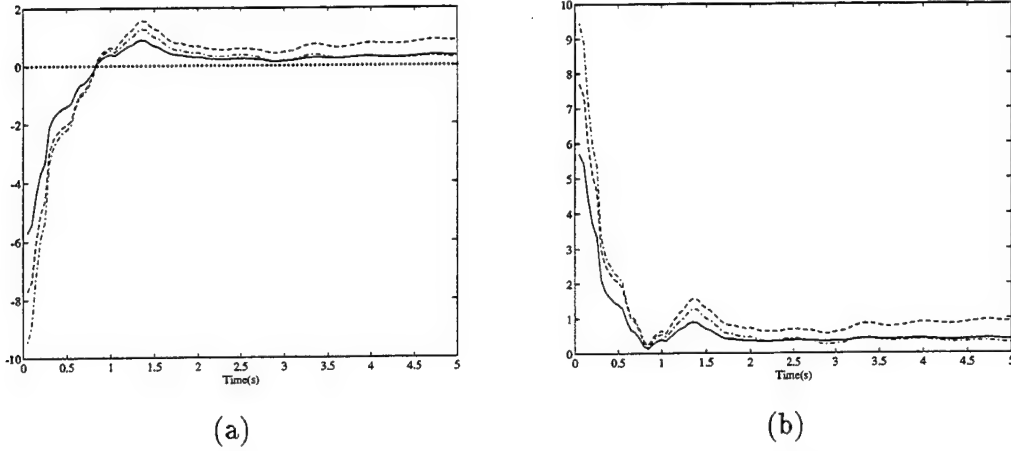


Figure 9: Bias and root mean-square error in the estimates of 3-D locations of close features, in the high signal to noise ratio case, from 50 Monte Carlo trials (solid line corresponds to the x coordinate, dashed line to the y coordinate, and dashed-dot line to the z coordinate). (a) Bias in Point 12, (b) root mean-square error in Point 12.

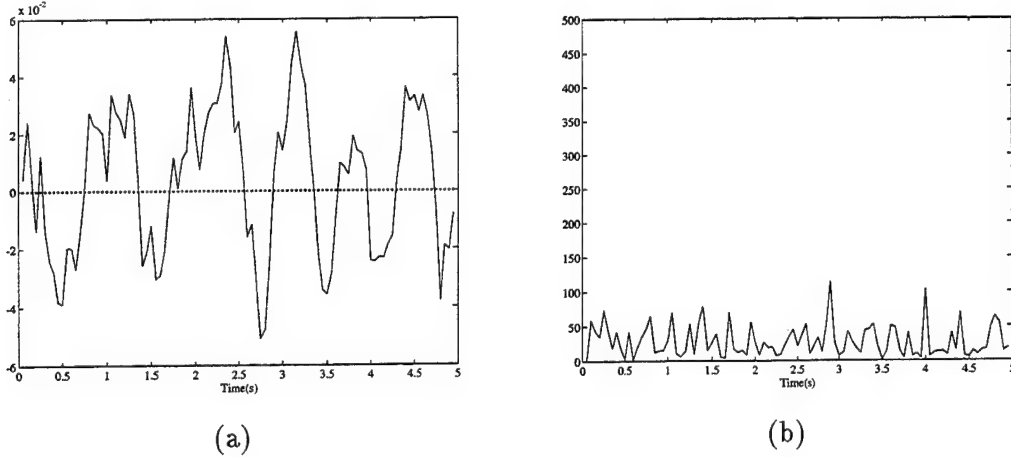


Figure 10: Estimate of the climbing-pitch rate ω_y and test statistic δ , in the low signal to noise ratio case, from 50 Monte Carlo trials. (a) ω_y , (b) δ .

6 Conclusions

This paper has presented a scheme for estimating the motion of a mobile robot as well as the relative positions of a set of discrete features. In particular, the algorithm employs different dynamic laws to capture different phenomena and utilizes various visual cues. It is shown that selective stabilization is possible. The use of an approximate kinetic law in achieving selective stabilization is justified. Schemes for the detection of the occurrence and disappearance of smooth rotation are investigated. Lastly, due to the separation of smooth rotation and oscillatory rotation, the 3-D locations of close features are easily estimated in a less perturbed frame of reference.

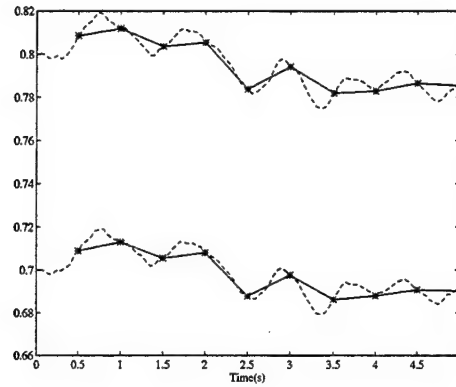
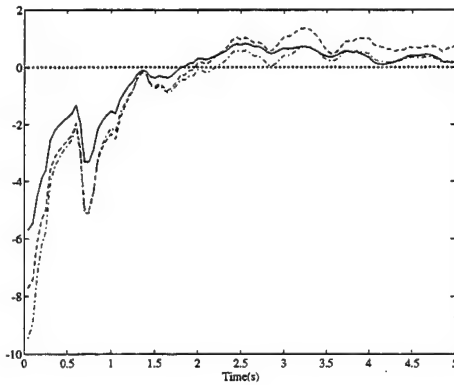
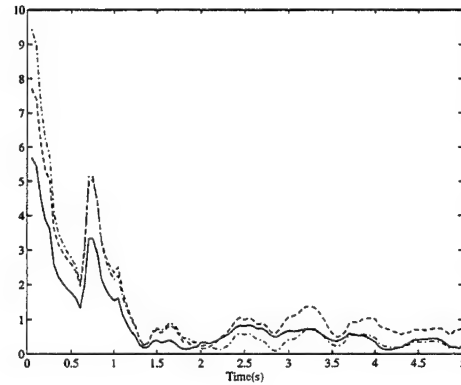


Figure 11: Vertical movements of distant points when the signal to noise ratio is low. Points 1 and 2 are displayed.

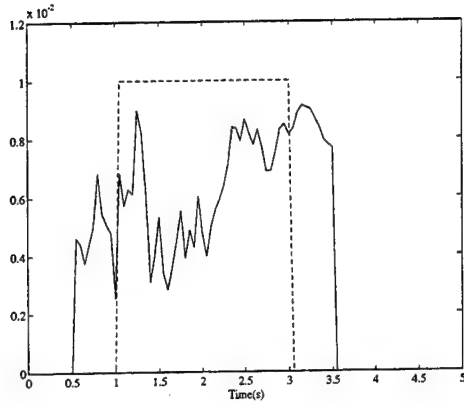


(a)

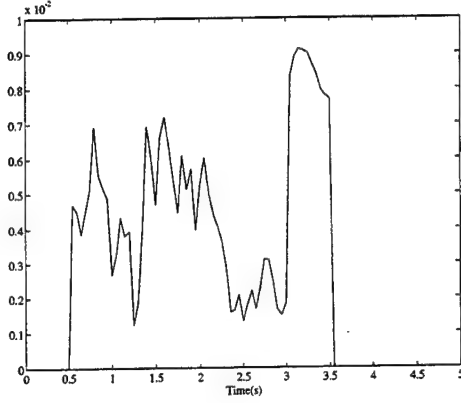


(b)

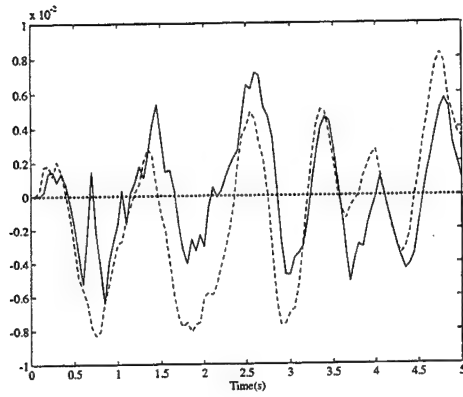
Figure 12: Bias and root mean-square error in the estimates of the 3-D locations of close features, in the low signal to noise ratio case, from 50 Monte Carlo trials (solid line corresponds to the x coordinate, dashed line to the y coordinate, and dashed-dot line to the z coordinate). (a) Bias in Point 12, (b) root mean-square error in Point 12.



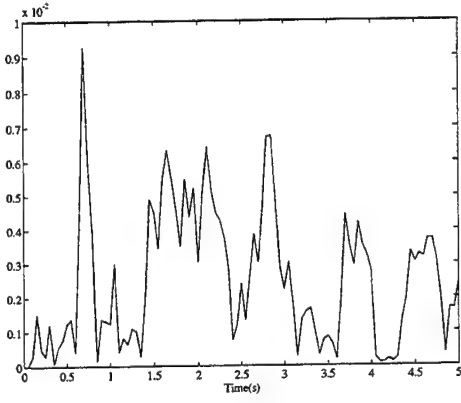
(a)



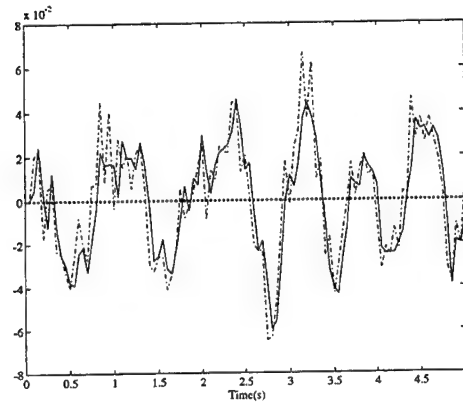
(b)



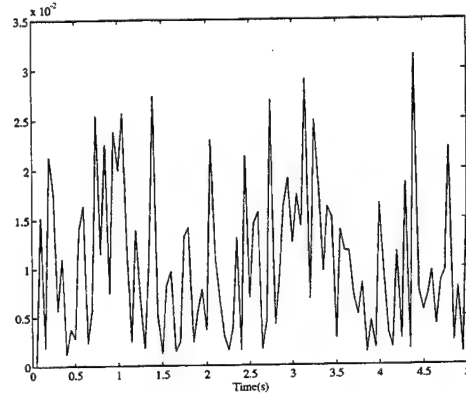
(c)



(d)



(e)



(f)

Figure 13: Estimates of climbing-pitch parameters, in the low signal to noise ratio case, from 50 Monte Carlo trials. (a) ω_{sy} : true (dashed line) and estimated (solid line), (b) ω_{sy} : root mean-square error, (c) θ : true (dashed line) and estimated (solid line), (d) θ : root mean-square error, (e) $\dot{\theta}$: true (dashed line) and estimated (solid line), (f) $\dot{\theta}$: root mean-square error.

References

- [1] G. Adiv. Determining three-dimensional motion and structure from optical flow generated by several moving objects. *IEEE Trans. on Pattern Analysis and Machine Intelligence*, 7:384-401, July 1985.
- [2] J.K. Aggarwal. Motion and time-varying imagery—An overview. In *Proc. of IEEE Workshop on Motion: Representation and Analysis*, pages 1-6, Kiawah Island, SC, May 1986.
- [3] P. Burt, R. Hingorani, and R.J. Kolczynski. Mechanisms for isolating component patterns in the sequential analysis of multiple motion. In *Proc. of IEEE Workshop on Visual Motion*, pages 187-193, Princeton, NJ, October 1991.
- [4] C.T. Chen. *Linear System Theory and Design*. Holt, Rinehart, and Winston, New York, 1984.
- [5] E.A. Desloge. *Classical Mechanics*, volume 2. New York: John Wiley & Sons, 1982.
- [6] J.Q. Fang and T.S. Huang. Some experiments on estimating the 3-D motion parameters of a rigid body from two consecutive image frames. *IEEE Trans. on Pattern Analysis and Machine Intelligence*, 6:545-554, September 1984.
- [7] A. Hady and D.A. Crolla. Theoretical analysis of active suspension performance using a four-wheel vehicle model. *Proc. of the Institution of Mechanical Engineers*, 203:125-135, 1989.
- [8] D.J. Heeger. Optical flow using spatiotemporal filters. *International Journal of Computer Vision*, 1:279-302, 1988.
- [9] J. Heel. Direct estimation of structure and motion from multiple frames. *AI Memo 1190*, MIT Artificial Intelligence Laboratory, March 1990.
- [10] B.K.P. Horn and B.G. Schunck. Determining optical flow. *Artificial Intelligence*, 17:185-203, August 1981.
- [11] J.K. Kearney, W.B. Thompson, and D.L. Boley. Optical flow estimation: An error analysis of gradient-based methods with local optimization. *IEEE Trans. on Pattern Analysis and Machine Intelligence*, 9:229-244, 1987.
- [12] Y. Liu and T.S. Huang. Vehicle-type motion estimation from multi-frame images. *IEEE Trans. on Pattern Analysis and Machine Intelligence*, 15:802-808, August 1993.

- [13] H.C. Longuet-Higgins. The reconstruction of a scene from two projections—Configurations that defeat the 8-point algorithm. In *Proc. of IEEE Conf. on Artificial Intelligence Applications*, pages 395–397, Denver, CO, December 1984.
- [14] H.C. Longuet-Higgins and K. Prazdny. The interpretation of a moving retinal image. *Proc. Royal Society London*, pages 385–397, 1980.
- [15] P. Michelberger, L. Palkovics, and J. Bokor. Robust design of active suspension system. *International Journal of Vehicle Design*, 14:145–165, 1993.
- [16] H.H. Nagel and W. Enkelmann. An investigation of smoothness constraints for the estimation of displacement vector fields from image sequences. *IEEE Trans. on Pattern Analysis and Machine Intelligence*, 8:565–593, 1986.
- [17] D. Sinclair, A. Blake, and D. Murray. Robust estimation of egomotion from normal flow. *International Journal of Computer Vision*, 13:57–69, September 1994.
- [18] R.Y. Tsai and T.S. Huang. Estimating three-dimensional motion parameters of a rigid planar patch iii: Finite point correspondences and the three view problem. *IEEE Trans. on Acoustics, Speech, and Signal Processing*, 32:213–220, April 1984.
- [19] A.M. Waxman, B. Kamgar-Parsi, and M. Subbarao. Closed-form solutions to image flow equations for 3D structure and motion. *International Journal of Computer Vision*, 1:239–258, 1987.
- [20] Y.S. Yao, P. Burlina, R. Chellappa, and T.H. Wu. Electronic image stabilization using multiple visual cues. In *Proc. of IEEE International Conference of Image Processing*, volume 1, pages 191–194, Washington, DC, 1995.
- [21] Z. Zhang and O.D. Faugeras. Three-dimensional motion computation and object segmentation in a long sequence of stereo frames. *International Journal of Computer Vision*, 7:211–241, August 1992.

Appendix A

We apply Lagrange's equations of motion to derive the oscillatory behavior of the four-wheel vehicle model in this appendix.

Consider Figures 2 and 3. Define the generalized coordinates, consisting of seven degrees of freedom, as

$$\mathbf{q} \stackrel{\text{def}}{=} (x_1, x_3, x_5, x_7, x_c, \theta, \phi)^T \quad (61)$$

Then Lagrange's equations of motion are written as follows [5]:

$$\frac{d}{dt} \left(\frac{\partial T}{\partial \dot{q}_j} \right) - \frac{\partial T}{\partial q_j} + \frac{\partial U}{\partial q_j} + \frac{\partial D}{\partial \dot{q}_j} = Q_j \quad j = 1, \dots, 7 \quad (62)$$

where $\{q_j, j = 1, \dots, 7\}$ constitute the generalized coordinates, T is the kinetic energy of the system, U is the potential energy, D is the dissipation function and Q_j 's represent the generalized forces acting on the system during vibration. In particular, as regards the behavior of $x_c, \theta, \dot{\theta}$, if the suspension system is of passive type, then the corresponding generalized force is assumed to be zero. We look at various energy terms in the following paragraphs.

• Kinetic energy

It is well known that the kinetic energy of a moving rigid body is equal to the sum of the translational and rotational kinetic energy. Therefore, taking into account the movements of the unsprung elements and oscillations of the sprung element, the kinetic energy is

$$T = T_B + T_w \quad (63)$$

where T_B is the kinetic energy contributed by the sprung element:

$$T_B = \frac{1}{2} M_B \dot{x}_c^2 + \frac{1}{2} I_{yy} \dot{\theta}^2 + \frac{1}{2} I_{zz} \dot{\phi}^2 \quad (64)$$

with M_B denoting the mass of the sprung element, and I_{yy} and I_{zz} being the moments of inertia with respect to the pitch and roll axes. T_w , on the other hand, is the kinetic energy contributed by the unsprung elements

$$T_w = \frac{1}{2} M_{wf} \dot{x}_1^2 + \frac{1}{2} M_{wf} \dot{x}_3^2 + \frac{1}{2} M_{wr} \dot{x}_5^2 + \frac{1}{2} M_{wr} \dot{x}_7^2 \quad (65)$$

- Potential energy

The potential energy U takes into account the influences of suspension springs and tires on a vehicle under going vibration. To obtain U , the deformations of suspension springs are first computed. They are approximated by

$$\begin{aligned} d_{f,r} &\approx x_c - T_{s,r}\phi + W_A\theta - x_1 \\ d_{f,l} &\approx x_c + T_{s,l}\phi + W_A\theta - x_3 \\ d_{r,r} &\approx x_c - T_{s,r}\phi - W_B\theta - x_5 \\ d_{r,l} &\approx x_c + T_{s,l}\phi - W_B\theta - x_7 \end{aligned} \quad (66)$$

Then assuming that linear relationships hold between the deformations and the forces generated by the springs, the potential energy is

$$U = U_S + U_T \quad (67)$$

where U_S is the energy stored in the suspension systems

$$U_S = \frac{1}{2}K_{f,r}d_{f,r}^2 + \frac{1}{2}K_{f,l}d_{f,l}^2 + \frac{1}{2}K_{r,r}d_{r,r}^2 + \frac{1}{2}K_{r,l}d_{r,l}^2 \quad (68)$$

and U_T is the energy stored in the tires,

$$U_T = \frac{1}{2}K_T \left[(x_1 - x_{01})^2 + (x_3 - x_{02})^2 + (x_5 - x_{03})^2 + (x_7 - x_{04})^2 \right] \quad (69)$$

- Dissipation function

The dissipation function accounts for the effects of the shock absorbers. Assuming that the forces generated by the shock absorbers vary linearly with the deforming rate, the dissipation function D is

$$D = \frac{1}{2}C_{f,r}\dot{d}_{f,r}^2 + \frac{1}{2}C_{f,l}\dot{d}_{f,l}^2 + \frac{1}{2}C_{r,r}\dot{d}_{r,r}^2 + \frac{1}{2}C_{r,l}\dot{d}_{r,l}^2 \quad (70)$$

After various energy terms have been considered, (62) is applied. The dynamics of θ and ϕ are then obtained.

Appendix B

In this appendix we analytically compare the performance of the approximate dynamic law of pitch and roll motion in (21) to the more complete dynamic law in (19). Equivalently, assume that the smooth rotation and oscillatory rotation are described by

$$\dot{\mathbf{x}}_0 = \mathbf{A}\mathbf{x}_0 + \mathbf{B}\mathbf{u}_{us} \quad (71)$$

where $\mathbf{x}_0 = (\omega_{sy}, \omega_{sz}, \mathbf{x}_{us}^T)^T$, \mathbf{A} and \mathbf{C} are defined in (31) and (32) respectively, while

$$\mathbf{B} = \begin{bmatrix} \mathbf{0}_{2 \times 2} & \mathbf{0}_{2 \times 10} \\ \mathbf{0}_{4 \times 2} & \mathbf{\Gamma}_{us} \end{bmatrix} \quad (72)$$

with $\mathbf{\Gamma}_{us}$ mentioned in (19). We study the behavior of the following linear systems.

$$\begin{cases} \dot{\mathbf{x}}_1 = \mathbf{A}\mathbf{x}_1 \\ \boldsymbol{\omega}_1 = \mathbf{C}\mathbf{x}_1 \end{cases} \quad (73)$$

where \mathbf{x}_1 consists of parameters related to smooth and oscillatory rotation, as defined in (30), and $\boldsymbol{\omega}_1$ denotes the measurable total angular velocity, again as defined in (30).

We employ a prediction-correction based scheme to separate the smooth and oscillatory rotation [4]:

$$\dot{\hat{\mathbf{x}}}_1 = \mathbf{A}\hat{\mathbf{x}}_1 + \mathbf{K}_1[\boldsymbol{\omega}_1 - \mathbf{C}\hat{\mathbf{x}}_1] \quad (74)$$

The resulting error $\tilde{\mathbf{x}}_1 = \mathbf{x}_0 - \hat{\mathbf{x}}_1$ then satisfies

$$\dot{\tilde{\mathbf{x}}}_1 = (\mathbf{A} - \mathbf{K}_1\mathbf{C})\tilde{\mathbf{x}}_1 + \mathbf{B}\mathbf{u}_{us} \quad (75)$$

By choosing an appropriate \mathbf{K}_1 , $\tilde{\mathbf{x}}_1$ will remain bounded as long as \mathbf{u}_{us} is bounded. Therefore, given reliable estimates of the total angular velocity, we can employ the approximate dynamic law (21) to achieve selective stabilization without much degradation.

REPORT DOCUMENTATION PAGE			Form Approved OMB No. 0704-0188	
Public reporting burden for this collection of information is estimated to average 1 hour per response, including the time for reviewing instructions, searching existing data sources, gathering and maintaining the data needed, and completing and reviewing the collection of information. Send comments regarding this burden estimate or any other aspect of this collection of information, including suggestions for reducing this burden, to Washington Headquarters Services, Directorate for Information Operations and Reports, 1215 Jefferson Davis Highway, Suite 1204, Arlington, VA 22202-4302, and to the Office of Management and Budget, Paperwork Reduction Project (0704-0188), Washington, DC 20503.				
1. AGENCY USE ONLY (Leave blank)	2. REPORT DATE August 1995	3. REPORT TYPE AND DATES COVERED Technical Report		
4. TITLE AND SUBTITLE Off-Road Navigation from Selective Stabilization		5. FUNDING NUMBERS DAAH04-93-G-0419		
6. AUTHOR(S) Y.S. Yao and R. Chellappa				
7. PERFORMING ORGANIZATION NAME(S) AND ADDRESS(ES) Computer Vision Laboratory Center for Automation Research University of Maryland College Park, MD 20742-3275		8. PERFORMING ORGANIZATION REPORT NUMBER CAR-TR-784 CS-TR-3509		
9. SPONSORING / MONITORING AGENCY NAME(S) AND ADDRESS(ES) U.S. Army Research Office P.O. Box 12211 Research Triangle Park, NC 27709-2211		10. SPONSORING / MONITORING AGENCY REPORT NUMBER ARO 32365.5-ma		
11. SUPPLEMENTARY NOTES The views, opinions and/or findings contained in this report are those of the author(s) and should not be construed as an official Department of the Army position, policy, or decision, unless so designated by other documentation.				
12a. DISTRIBUTION / AVAILABILITY STATEMENT Approved for public release; distribution unlimited.		12b. DISTRIBUTION CODE		
13. ABSTRACT (Maximum 200 words) This paper studies the problem of selective stabilization, defined here as the separation of rotation components due to smooth rotation and oscillatory rotation. In applications to off-road navigation, in addition to the desired smooth attitude change, a vehicle undergoes high frequency vibration. We consider both kinematic and kinetic models suitable for capturing these phenomena and achieving their separation. Our approach uses various dynamic laws to model the behavior of the vehicle, and relies on Extended Kalman Filters for the estimation. Multiple visual cues are exploited to obtain the rotational parameters. A scheme for detecting the occurrence and disappearance of smooth rotation is devised. Appropriate dynamic laws are employed to achieve selective stabilization. Based on the selective stabilization, 3-D locations of close feature points are estimated in a stabilized frame of reference, thus providing more useful information. Synthetic experiments for different scenarios using the proposed approach show promising results.				
14. SUBJECT TERMS Selective stabilization, motion analysis, structure from selective stabilization, kinematic and kinetic models			15. NUMBER OF PAGES 34	
			16. PRICE CODE	
17. SECURITY CLASSIFICATION OF REPORT UNCLASSIFIED	18. SECURITY CLASSIFICATION OF THIS PAGE UNCLASSIFIED	19. SECURITY CLASSIFICATION OF ABSTRACT UNCLASSIFIED	20. LIMITATION OF ABSTRACT UL	